HEM and HRM accuracy comparison for the simulation of CO_2 expansion in two-phase ejectors for supermarket refrigeration systems

Michal Palacz[a,*], Michal Haida[a], Jacek Smolka[a], Andrzej J. Nowak[a], Krzysztof Banasiak[b], Armin Hafner[c]

[a] *Institute of Thermal Technology, Silesian University of Technology, Konarskiego 22, 44-100 Gliwice, Poland*
[b] *SINTEF Energy, Kolbjørn Hejes v. 1D, Trondheim, 7465, Norway*
[c] *Department of Energy and Process Engineering, NTNU, Kolbjørn Hejes vei 1d, Trondheim, 7465, Norway*

Abstract

In this study, the accuracies of the homogeneous equilibrium (HEM) and homogeneous relaxation models (HRM) were compared. Both models were implemented in the *ejectorPL* computational tool. The HEM and HRM were used to simulate the carbon dioxide flow in ejectors that were designed for supermarket refrigeration systems. The model accuracy was evaluated by comparing the computational results with the experimental data. The discrepancy between the measured and computed motive nozzle mass flow rates was analysed. In addition, the difference between the experimental and computational mass entrainment ratios was calculated. The operating regimes in this study ranged from 47 bar to 94 bar and from 6°C to 36°C for the pressure and temperature, respectively. The model accuracy strongly depends on the distance between the operating regime and the critical point of the refrigerant. The discrepancy for the selected operating regimes ranged from 0.3% to 43.3% and 0.7% to 42.0% for HEM and HRM, respectively. For lower pressures and temperatures, the HRM has higher accuracy than the HEM. The errors of the HRM results were approx. 5% lower than those of the HEM results. The accuracy improvement of the HRM was considered unsatisfactory. The low accuracy improvements were possibly caused by the relaxation time formulation in the homogeneous relaxation model.

Keywords:

Todo list

Nomenclature

c_p	specific heat, kJ·kg^{-1} K^{-1}
H	total enthalpy, kJ·kg^{-1}
h	specific enthalpy, kJ·kg^{-1}
k	effective thermal conductivity, W m^{-1}K^{-1}
p	pressure, Pa
$\dot{m}$	mass flow rate, kg·s^{-1}
s	specific entropy, kJ·kg^{-1} K^{-1}
T	temperature, K
$\boldsymbol{U}$	velocity vector, m·s^{-1}
t	time, s
x	actual vapour quality, –

Greek Symbols

α	volume fraction of vapour, -
χ	mass entrainment ratio, -
δ	relative difference, %
η	overall ejector efficiency, %
μ	dynamic viscosity, Pa·s

*Tel.: +48 322372810; fax: +48 322372872
michal.palacz@polsl.pl

ϕ	dimensionless pressure difference, -	i	number
ρ	density, kg·m^{-3}	in	inlet
τ	stress tensor, N·m^{-2}	l	liquid phase
θ	relaxation time, s	ml	metastable liquid
Subscripts		mn	motive nozzle
c	critical parameter	out	outlet
CFD	computed value	s	saturation
DIF	diffuser	sn	suction nozzle
eq	equilibrium	sv	saturated vapour
EXP	measured value	v	vapour phase

1. Introduction

Throttling losses significantly affect the performance of refrigeration systems. That relation is so strong that throttling is called the *internal haemorrhage of the refrigeration process* in the literature [1]. Throttling losses are relatively high in refrigeration systems that operate in high-pressure conditions. CO_2 (R744)-based refrigeration units are good examples of such systems. Because of the relatively low critical temperature of carbon dioxide, R744 units often operate in the transcritical mode. Consequently, these systems have lower coefficients of performance (COP) than the HFC or CFC systems, particularly for high ambient temperatures. To overcome that drawback, two-phase ejectors were introduced and applied to the expansion work recovery. Therefore, the throttling losses are reduced, and the COP of the system is improved. The authors such as [2] compared traditional AC carbon dioxide transcritical system with the system equipped with ejector. The published results showed that the application of the ejector in that system improved its COP by more than 16%. The similar improvements were reported by [3]. In that work, the prototype ejector was implemented into the refrigeration system. The authors of that papers proved that the expansion work was recovered up to 14.5%. In consequence, the COP of that system was improved by 18%. The recent review papers also showed that the ejector application in transcritical CO_2 systems is the most effective way to improve the COP of such system in warm climates, see [4, 5, 6]. The most recent development of the CO_2 ejector systems were also experimentally investigated by [7] or [8]. Liu et al. (2016) [8] experimentally investigated the controllable ejector for various systems loads. The results of that investigation showed that there are possibilities to control the system load of the refrigeration system. Alternative approach was tested by the authors of [7]. In that paper the multiejector block was implemented in parallel compression system. The various size ejectors were installed in the mentioned multiejector block. Consequently, the cooling capacity of the system was controlled by the parallel work of the installed ejectors. Both mentioned authors reported the COP increase for the considered operating regimes. Moreover, it is worth mentioning that both investigations were performed for relatively high ambient temperatures.

The two-phase ejector design is relatively simple. This device is an assembly of four key parts: motive nozzle, suction nozzle, mixer and diffuser. Each part of the device is responsible for a slightly different process. The shape of each part significantly affects the ejector performance. Hence, the analysis of the ejector shape and its performance is an important topic in many scientific investigations. Recently, [9] experimentally mapped the efficiency of the ejectors that were installed in the multi-ejector module. The authors of [10] numerically investigated the performance of the ejectors installed in the mentioned module and compared it with the controllable ejector performance introduced and investigated by [11, 12]. The ejector efficiency definitions were also used as the objective function for the ejector shape optimisation [13]. Moreover, considering the results presented in [14, 13], the ejector shape is crucial for the device performance. Similar findings were reported for the ejectors for different working fluids, e.g., [15]. For the experimental analysis of the ejectors, the device must be first manufactured, and the mathematical modelling of the fluid seams is a good alternative in the case of the ejector prototyping

and designing. Hence, various models were recently developed to simulate the refrigerant flow in the ejector. Nevertheless, the accuracy of the considered mathematical model should be evaluated first to define the model application range.

One of the first dimensionless models for the ejector was introduced by [16]. The author of that work used the developed model to show the increase in COP of the refrigeration system after the ejector implementation. Then, more complex 1-D ejector models were developed. [11] introduced this model to analyse the ejector performance. The model concept was to apply different models for each ejector section. Hence, the group of submodels was used to calculate values such as the mass entrainment ratio, pressure lift and ejector efficiency. In this approach, the isentropic efficiency of the motive nozzle was initially assumed. The model results of the mentioned authors were consistent with the experimental data. Nevertheless, the efficiencies of the ejector sections were assumed in that model.

A more complex model was developed by [17]. Similar to [11], the sub-models were applied for various ejector parts. However, the more sophisticated two-phase flow model was used. The author modelled the CO_2 expansion in the diverging part of the motive nozzle by applying the Delayed Equilibrium Model (DEM) [18], which was enhanced with the Homogeneous Nucleation Theory (HNT) [19]. Moreover, [20, 9]used that approach for the ejector design. The mentioned one-dimensional models can be effectively used to predict the ejector performance. However, because of its simplicity, the more complex CFD models should be used to investigate the flow field in ejectors. The recent modelling approaches for CO_2 ejectors were briefly described in [21].

[22] introduced the CFD model for the ejectors in combined cooling system. The authors of that model used the commercial Ansys Fluent solver to simulate the refrigerant flow in the device. The discrepancies between experimental and computed values for the area ratio in [22] were below 10%. In this approach, the turbulence was modelled with the k - ϵ model, and NIST REFPROP [23] libraries were used to obtain the actual fluid properties. However, that model was formulated for R141b.

The numerical model that was developed for CO_2 flow in the ejectors was presented in [24]. Similar to the previously mentioned approach, [24] uses the Ansys Fluent solver and REFPROP libraries. Moreover, the fast in-house developed approximations of actual-fluid libraries were implemented in Ansys Fluent using the User Defined Functions (UDFs) capability. The Realisable $k-\epsilon$ [25] model was used for the turbulence. The [24] model was validated for the single-phase R141b ejector and two-phase R744 (carbon dioxide) ejector. [26]also modelled the carbon dioxide flow in the two-phase ejector. Unlike [24] and [22], the free OpenFOAM solver was used to simulate the fluid flow. Moreover, the authors of [26] reduced the computational domain to 2-D axisymmetric. The actual fluid properties were obtained from the TEMO-Media library. Both, [24] and [26]used the homogeneous equilibrium model (HEM) for the two-phase flow. The differences between the predicted and simulated motive nozzle mass flow rates were less than $\pm$10% in the presented models.Nevertheless, the range of motive nozzle operating conditions was relatively narrow. The considered operating regimes were distributed near the carbon dioxide critical point. [27] investigated the accuracy of the HEM approach for the two-phase CO_2 ejectors. The results of [27] showed the range of HEM applications.The significant lack of fidelity of this tow-phase flow model was noted. According to the mentioned study, the accuracy of the HEM decreased with the decreasing pressure and temperature, namely for the operating conditions far from the critical point. This rapid increase in difference between experimental and computed values is caused by the metastable effects during the fluid expansion, which are neglected in HEM. To include the metastable effects in the numerical model, the more complex two-phase flow model must be implemented.

Alternatively to HEM, the homogeneous relaxation model (HRM) was applied for the CO_2 flow simulations in the ejectors. In this approach, the relaxation time is included to calculate the actual vapour quality [28]. Hence, the metastable effects are considered in the model. The relaxation time for the HRM model was defined by [29]. The authors of [29] determined the relaxation time for CO_2 and compared the obtained numerical results with the experimental data of [30]. The relaxation time definition in [29] was successfully used by [31] for the two-phase ejector analysis. The author of [31] used the CFD model that [32] introduced. [31] used the OpenFOAM as the solver, and similarly to [22] and [24], [31] used the NIST REFPROP for the real fluid properties. In [31], the measured and computed pressure recovery values were compared to assess the modelling accuracy. The nozzle operating pressure was 95-105 bar. In addition, the analysis was performed for various mixing section lengths with or without the internal heat exchanger (IHX). Unfortunately, the presented results showed significant discrepancy between the model and the experiment. In some cases, the presented differences were above 20%. Moreover, the

range of investigated operating conditions was too narrow to properly evaluate the HRM fidelity for the ejector simulation for the refrigeration systems.

The HRM approach was also used for different applications where the CO_2 two-phase flow occurs. [33] and [34] simulated the leakage of CO_2 from the pipelines in Carbon Capture and Storage (CCS) systems. Both papers provided notably detailed and valuable information about the model description and performance. However, similarly to [31], [33] and [34] investigated a small number of operating conditions. Moreover, the feed pressure was significantly higher than the CO_2 critical point.

To properly assess the limitations and performance of the HRM for refrigeration systems, particularly supermarket refrigeration systems, a deeper analysis is needed. Hence, an analysis analogical to that introduced by [27] is presented in this paper. The HRM formulation for CO_2 expansion in supersonic nozzles was adapted from [29]. Then, it was applied in the computational tool *ejectorPL*, which was previously used for the HEM accuracy analysis. In this study, *ejectorPL* was applied to evaluate the HEM and HRM accuracy for the typical operating regimes of supermarket CO_2 The motive nozzle operating conditions for the accuracy assessment were 47 bar to 95 bar for the pressure and 6°C to 35°C for the temperature. The computational and experimental results, which were obtained during the ejector test campaign at SINTEF Energy Research, Trondheim, Norway, were compared. According to our best knowledge, such an extensive HRM analysis has not yet been published.

2. Model description

2.1. HEM model

As briefly mentioned in Section 1, HEM was successfully used to model the carbon dioxide expansion. In the HEM approach, a set of governing equations must be solved. Hence, the mass momentum and energy conservation equations for the steady state have the following form:

$$\nabla \cdot (\rho \boldsymbol{U}) = 0 \tag{1}$$

$$\nabla \cdot (\rho \boldsymbol{U}\boldsymbol{U}) = -\nabla p + \nabla \cdot \tau \tag{2}$$

$$\nabla \cdot (\rho \boldsymbol{U} H) = \nabla \cdot (k \nabla T + \tau \cdot \boldsymbol{U}) \tag{3}$$

The mixture total enthalpy is defined as the sum of the specific enthalpy and kinetic energy of the fluid (Eq. 4).

$$H = h + \frac{U^2}{2} \tag{4}$$

Moreover, in HEM, the thermodynamic and mechanical equilibrium between both phases is assumed. In consequence, all thermodynamic and transport properties of the fluid are functions of the pressure and the specific enthalpy (Eq. 5).

$$\{\rho, c_p, k, \mu\} = f(p, h) \tag{5}$$

As it can be seen, the time derivatives in Eqs. (1)-(3) were neglected. Therefore, all the computations were performed for the steady state. Moreover, the heat transfer through the ejector walls was neglected in this study. It is also worth mentioning that the shape of the considered ejectors was axisymmetric. Hence, the computational domain was simplified to 2-D axisymmetric. Analogical assumptions were used in the previous papers of the authors, e.g. [10, 27].

2.2. HRM model

In HRM, the mechanical equilibrium between liquid and vapour phases is assumed as in HEM. Moreover, the non-equilibrium phase change is considered. The non-equilibrium phenomenon is accounted by the relaxation time of the thermodynamic equilibrium. The actual vapour quality was defined by [28] as follows:

$$\frac{\partial(\rho U x)}{\partial z} = \rho \frac{\bar{x} - x}{\theta} \tag{6}$$

The relaxation time (θ) definition was formulated by [28] according to the Moby Dick experiments (Eq. (7)).

$$\theta = \theta_0 \alpha^a \phi^b \tag{7}$$

The dimensionless pressure difference (ϕ) was originally defined by [28]. Then it was adapted for the supercritical parameters by [29]. In consequence, the ϕ was defined as follows:

$$\phi = \left| \frac{p_{sat(s_{MN,in})} - p}{p_c - p_{sat(s_{MN,in})}} \right| \tag{8}$$

The α in Eq. (7) was defined similar to [32]:

$$\alpha = \frac{\rho_{sl} - \rho}{\rho_{sl} - \rho_{sv}} \tag{9}$$

The coefficients and exponents θ_0, a and b for CO_2 were presented in [29]. These authors used the HRM to analyse the carbon dioxide flow through the ejector nozzle. The nozzle geometry and experimental data in [29] were obtained from the experimental CO_2 supersonic nozzle in [30]. Finally, Eq. (7) with the coefficients and exponents that [29] introduced can be rewritten as follows:

$$\theta = 2.15 \times 10^{-7} \alpha^{-0.54} \phi^{-1.76} \tag{10}$$

Consequently, the mixture density and specific enthalpy must be computed again in the following equations:

$$\frac{1}{\rho} = \frac{x}{\rho_{sv}} + \frac{1-x}{\rho_{ml}(p, h_{ml})} \tag{11}$$

$$h = x h_{sv}(p) + (1-x) h_{ml} \tag{12}$$

2.3. Computational procedure

The described two-phase models were implemented to the *ejectorPL* script. Initially, only the HEM formulation was available with that script. Originilaly the mathematical model developed by [24] was implemented in the*ejectorPL*. That approach was used for the HEM accuracy analysis ([27]), shape optimisation of the supermarket CO_2 ejectors ([13]), analysis of the performance of the controllable ejectors ([10]), liquid ejectors analysis ([35]), and analysis of the swirl motion ejectors ([36]). In each of mentioned case the HEM approach was used. The realiabity of the results was sufficient enough to use the numerical results for the ejectors prototyping, manufacturing and finally installing them in the industrial supermarket refrigeration system [37]. The most important benefit of the application *ejectorPL* for such analysis or model accuracy analysis was that the computational procedure was exactly identical for all considered ejector designs or operating conditions. The *ejectorPL* script was described in detail in ([27]).

The *ejectorPL* script is a combination of the pre-processor (Ansys ICEM CFD) and Ansys Flunet solver [38]. The schema of the *ejectorPL* platform is presented in Fig. 1.The post-processing procedure was developed in-house. The generated structural numerical grids consisted of approx. 10 000 hexahedron elements. The generated mesh was refined in the region of high gradients, namely at the motive nozzle outlet and the premixing section of the ejector. Similar numerical grids were used by the authors in various CO_2 ejectors investiagtions, e.g. [7] or [27]. The real fluid properties were obtained by the commercial NIST REFPROP libraries [23]. The wall roughness was set to 2 μm [39]. That value was related to the roughness declared by ejector manufacturers. The mathematical model of [24] was enhanced to HRM optional computations. The solving procedure was set up to simulate the fluid flow for only HEM. After the HEM results were obtained, the HRM was activated. As a result of the HRM activation, the additional User Defined Scalar (UDS) was activated [38], which was used to calculate the actual vapour quality in Eq. (6). The relaxation time θ for the HRM computations was calculated according to Eq. (10), which [29] presented. The convergence criterion was reached when the mass flow rate imbalance was below 1% of the motive nozzle mass flow rate. Moreover, to reduce the computational time, the genuine procedure for the solver initialisation was used. In consequence, the computational time was 40 minutes per case. All computations were performed using the Institute Thermal Technology, Gliwice, Poland, computing cluster.

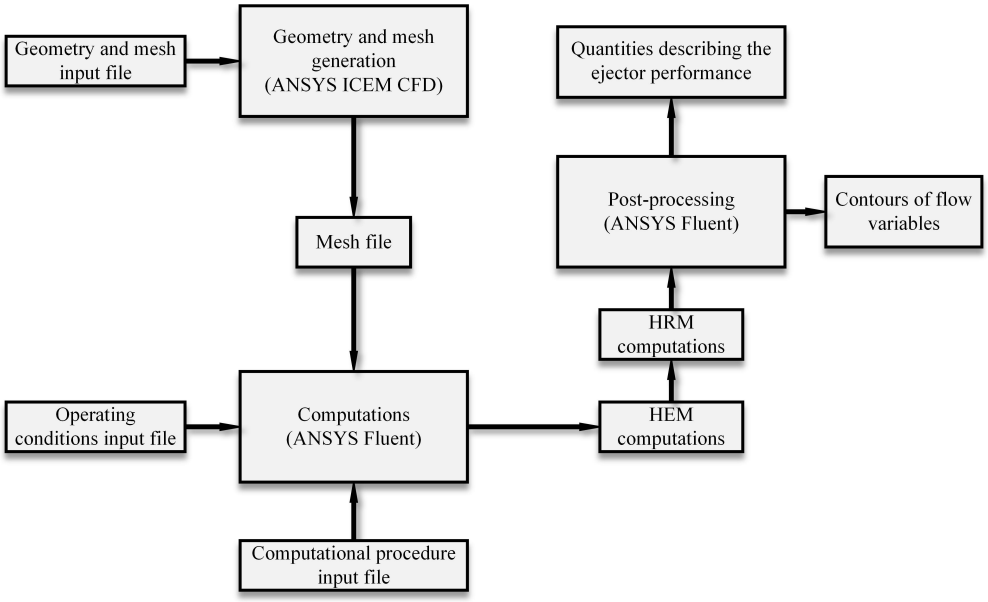

Figure 1: Flowchart of the *ejectorPL* script

3. Experimental results

The experimental data, which were used as the operating conditions for the ejectors and the measured mass flow rates, were captured during the ejector test campaign in SINTEF Energy Research. The experimental rig was constructed as the actual supermarket refrigeration system, which was equipped with a multi-ejector rack. The rig was also used by [9] to map the ejector performance. A detailed description of the experimental facility can be found in [9].

The experimental refrigeration system was rated for 70 kW at a 35°C gas cooler temperature. In that system, the multi-ejector module, which consisted of four vapour ejectors EJ1-EJ4, was installed. The cooling capacity of this system was controlled by the parallel work of these ejectors. Different sizes of ejector motive nozzles were used. EJ1 was originally designed using the [17] model (see [9]). Then the ejectors EJ2-EJ4 were scaled-up version of the EJ1. The dimensions of the considered motive nozzles are presented in Table 1.

Table 1: Dimensions of the shape of the considered motive nozzles, [9, 13, 35]

Dimension	**EJ1**	**EJ2**	**EJ3**	**EJ4**
Inlet diameter, mm	3.80	3.80	3.80	3.80
Throat diameter, mm	1.00	1.41	2.00	2.83
Outlet diameter, mm	1.12	1.58	2.24	3.16
Converging angle, °	30.00	30.00	30.00	30.00
Diverging angle, °	2.00	2.00	2.00	2.00

The test facility was equipped with a high-quality temperature and pressure sensor. The PT1000 calibrated thermocouples and calibrated piezoelectric elements were used for the temperature and pressure measurements, respectively. Moreover, the Coriolis-type mass flow metres were installed in the system. The accuracy of the equipment was: $\pm 0.5\times10^{-3}$ kg s^{-1}, $\pm$ 2.5$\times10^{4}$ Pa and $\pm$ 0.6 K, respectively. The entire experimental rig was described by [7] in detail.

The range of operating regimes in this study was typical for the supermarket refrigeration units that are installed in Northern and Southern Europe (see [40]). The motive nozzle inlet parameters were 50 bar to 94 bar for the pressure and 6°C to 34°C for the temperature. The suction nozzle operating conditions were characteristic

for food storage purposes. For all considered cases, the suction pressure was 27-31 bar, and the temperature was 1-6°C. A detailed list of the considered ORs is presented in Table 2. The presented operating regimes are listed from the lowest to the highest motive nozzle inlet specific enthalpy. In addition, the measured motive nozzle mass flow rate and χ are presented in Table 2.

Table 2: Operating regimes for the HEM and HRM accuracy evaluation

OR No.	Motive nozzle		Suction nozzle		Outlet	$\dot{m}_{MN}$, kg/s	χ, -
	p, bar	t, °C	p, bar	t, °C	p, bar		
1	53.93	6.33	27.30	5.70	34.23	0.099	0.30
2	58.41	10.00	27.82	4.56	34.83	0.103	0.07
3	47.82	9.79	27.93	8.49	31.89	0.172	0.08
4	59.30	17.67	28.49	5.42	33.87	0.041	0.15
5	58.43	17.69	28.45	1.98	31.01	0.040	0.33
6	61.79	20.27	29.93	3.58	33.87	0.072	0.26
7	64.79	22.09	28.01	2.48	33.77	0.037	0.22
8	66.62	22.38	27.87	1.78	32.88	0.072	0.31
9	66.51	22.41	28.21	2.21	34.85	0.072	0.19
10	75.10	23.70	32.01	5.98	37.34	0.047	0.28
11	80.62	26.25	31.58	5.34	38.48	0.089	0.28
12	87.86	28.40	31.55	5.51	38.29	0.097	0.33
13	78.45	28.56	31.72	5.71	38.28	0.073	0.36
14	75.79	28.07	28.17	2.58	36.80	0.089	0.28
15	91.91	30.98	31.41	5.28	38.24	0.095	0.35
16	76.56	28.34	27.33	0.86	32.87	0.067	0.42
17	86.04	31.33	27.32	0.46	32.90	0.079	0.42
18	94.46	35.28	27.21	2.60	32.85	0.084	0.42

4. HEM and HRM accuracy

The numerical analysis was performed for the HEM and HRM models. The relaxation time in the HRM was calculated according to the formulation proposed by [29]. The computational results were compared with the experimental data. Namely, the motive nozzle mass flow rates that were experimentally and numerically determined were compared. A dimensionless factor called the mass entrainment ratio (χ),which was defined as the ratio between the sucked mass flow rate and the driving mass flow rate (Eq. 13), directly affects the ejector efficiency (η_{EJ})), which was defined by [41]. Hence, the discrepancy between the measured and computed χ was assessed for both two-phase flow models.

$$\chi = \frac{\dot{m}_{SN}}{\dot{m}_{MN}} \tag{13}$$

As mentioned, the computational and experimental motive nozzle mass flow rates were compared. To evaluate the discrepancy, the following definition was used:

$$\delta = \left(1 - \frac{\dot{m}_{MN,CFD}}{\dot{m}_{MN,EXP}}\right) \cdot 100 \tag{14}$$

The calculated errors using the above definition are presented in Fig. 2. In Fig. 2, δ for the HEM and HRM is presented in the scale of the reduced motive nozzle inlet pressure and reduced temperature. In addition, the discrepancy definition and the CO_2 critical point are presented in that figure. The difference between the predicted and measured χ for the ORs in Table 2 is presented in Fig. 3.

The results presented in Fig. 2 clearly show the high dependency of the model accuracy and the proximity to the critical point. The model accuracy evaluation in Fig. 2 shows that the model fidelity decreases with decreasing

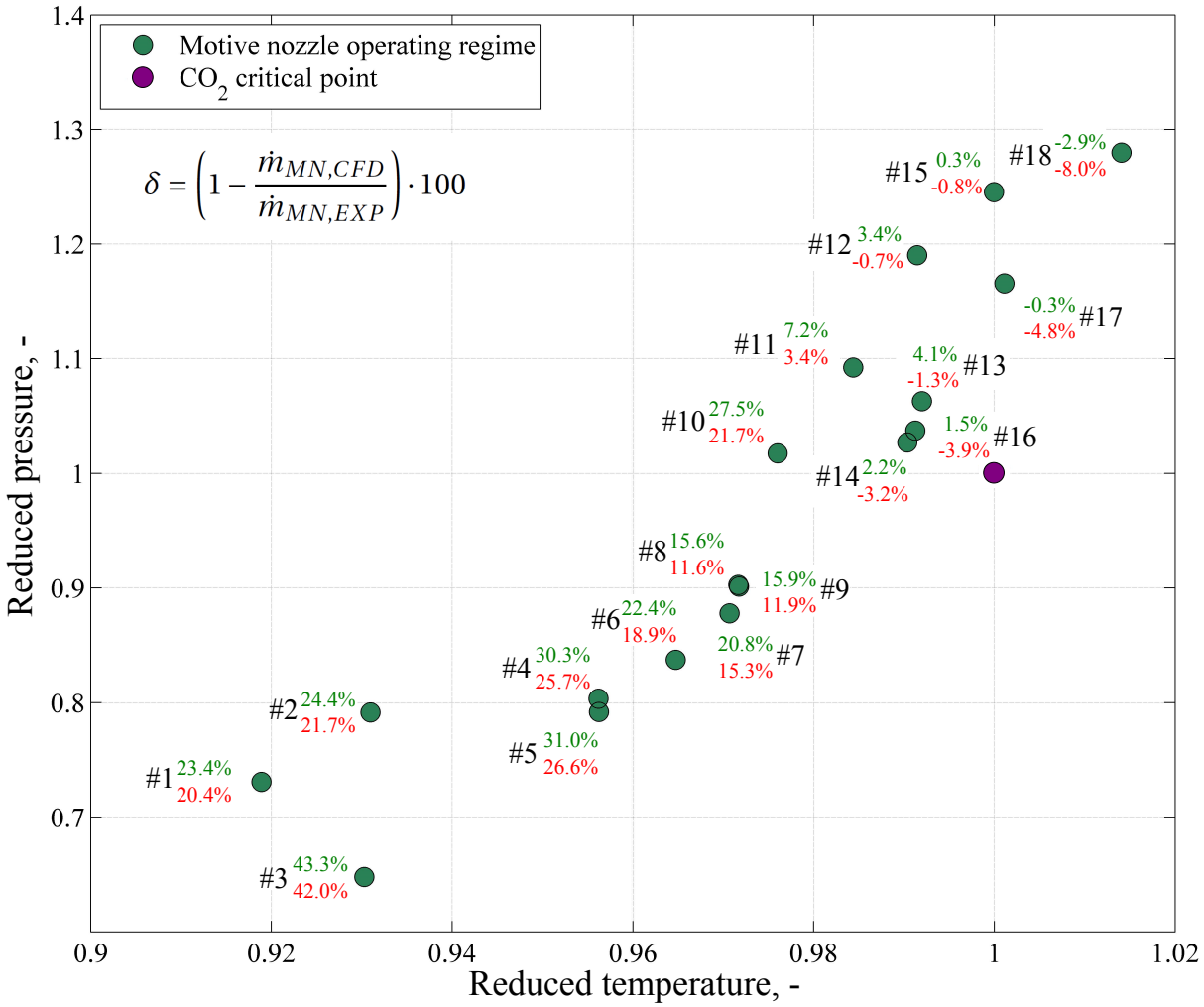

Figure 2: HEM (green) and HRM (red) accuracy vs operating conditions in the reduced pressure and temperature scale

primary stream specific enthalpy. For the ORs such as #11 - #16, the difference between the computed and measured values was at an acceptable level, i.e., ± 10 %. Moreover, the error of χ in Fig. 3 was in the same level for points #12 - #13. However, the predicted mass entrainment ratio for OR #14 was significantly underestimated. For OR #14, the pressure lift (difference between the suction nozzle pressure and the outlet pressure) is much higher than for those of operating regimes #12 - #13. A similar trend was observed for operating regime #7. Comparing ORs #6, #7 and #8, we observe that the result accuracy was the worst for operating regime #7, which had the highest pressure lift. This inconsistency between the motive nozzle mass flow rate and χ error should be considered, particularly if the model is used to evaluate the ejector performance. The results in Figs. 2 and 3 show that the motive nozzle mass flow rate prediction and χ prediction are not directly dependent. The fidelity of the mass entrainment ratio prediction is related by additional uncertainty. The suction nozzle mass flow rate simulations are also affected by the turbulence model or the the wall roughness defined in the model.

Further analysis of the ORs in Fig. 2 shows that for the ORs above the critical point, the HEM was more accurate than the HRM. For operating regimes such as #17 or #18, the error of the HRM computations was almost two times higher than that of the HEM approach. The fluid expansion that began from such points ended in the two-phase flow region with negligible metastable effects. The relaxation time that was calculated using Eq. (10) is significantly shorter than that calculated for the low-pressure ORs. Nevertheless, the relaxation time introduced in the HRM

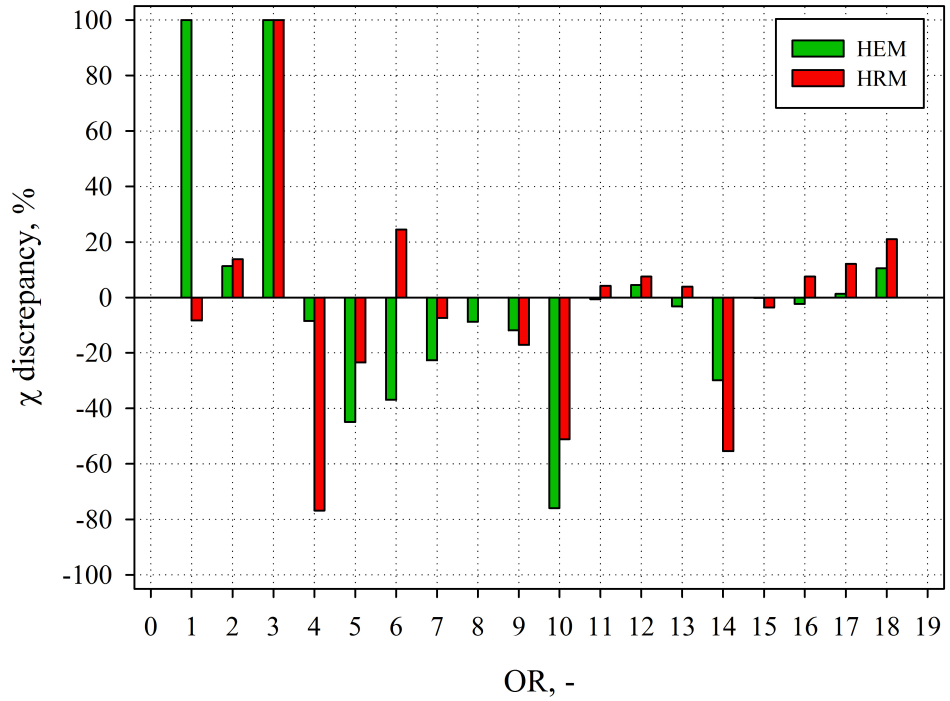

Figure 3: Accuracy of the χ prediction for the HEM (green) and HRM (red) model

model affects the process and results in the overestimated mass flow rate.

The simulated higher motive nozzle mass flow rates increase the model accuracy when the HRM is applied for ORs #1, #3 a or #5. Compared to the HEM results for these points, the relaxation model increased the fidelity of the computations by approximately 4%. An even higher increase in accuracy was noted for point #7. Moreover, in the operating regimes where the motive nozzle inlet pressure was approximately 60 bars, the highest accuracy improvements were recorded. The model fidelity was also improved for χ. For OR #1, the suction nozzle mass flow rate was zero for the HEM and predicted with an acceptable error for the HRM. Nevertheless, the predicted suction nozzle mass flow rate was 0 for the motive nozzle inlet pressure below 50 bars.

The results for ORs #11 and #13 show that the relation between the model accuracy and the inlet temperature is stronger than that between the accuracy and the inlet pressure. The difference in pressure of these two points is approximately 0.03 Pa, but the reduced temperature difference is below 0.001 K. Nevertheless, the notable decrease in model accuracy was noted for the ORs with lower temperature. Similar findings are observed for the HEM results for ORs #13 and #14. The almost negligible change in temperature resulted in the decrease in HEM fidelity by 0.7%. The dependence of the model accuracy on the motive nozzle inlet temperature was reported in the literature ([26], [33] and [27]). Consequently, the data in this paper are consistent with the recent studies.

The higher mass flow rates obtained with HRM were caused by the lower vapour quality of the fluid in the motive nozzle throat. In consequence, the density of the expanding fluid was notably higher in this ejector part. The lower vapour quality obtained with HRM resulted from the delay of the fluid evaporation. This delay was caused by the relaxation time (Eq. (10)). To illustrate the evaporation delay, the vapour quality profiles along the ejector axis (from the motive nozzle throat to the mixer inlet) were calculated for HEM and HRM and shown in Figs. 4 and 5. The fluid evaporation began earlier for the HEM formulation. In the case of the HEM, the fluid evaporation began at approximately the motive nozzle throat. For the low inlet temperature and pressure conditions, e.g., OR #1, the evaporation began in the diverging part of the motive nozzle that was relatively far from the motive nozzle throat. For the ORs near the critical point, e.g., OR #16, the tendency was identical to that in the previous case.

However, in Fig. 5, the difference of the beginning of the phase change for HEM and HRM was significantly lower than that for OR #1 in Fig. 4. Moreover, the noted vapour quality for OR #16 was significantly higher than that for OR #1. Consequently, more vapour CO_2 flowed into the mixing section. In the case of OR #16, the thermodynamic equilibrium was reached at approximately the mixer inlet, which was similar for OR #1.

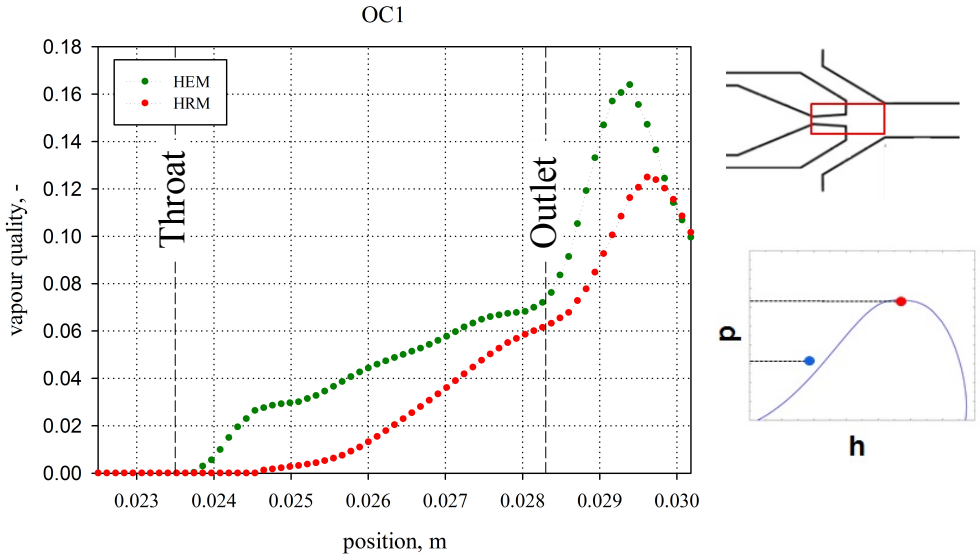

Figure 4: Vapour quality profiles for HEM/HRM for OR #1 (left), the considered ejector part (marked in red) and the OR position with respect to the critical point (right)

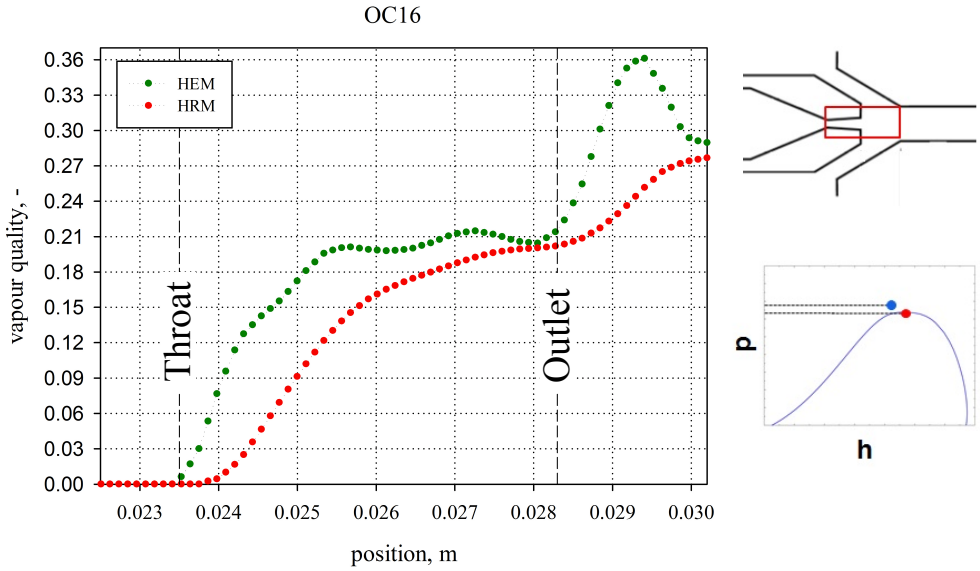

Figure 5: Vapour quality profiles along the ejector axis for HEM/HRM for OR #16 (left), the considered ejector part (marked in red) and the OR position with respect to the critical point (right)

As previously mentioned, the HRM vapour quality affects the computed density. In consequence, the other flow field variables are also affected. The HRM had a slightly lower computed velocity than the HEM. The comparison of the velocity magnitude fields in the motive nozzle for HEM and HRM is presented in Fig. 6. The velocity

near the nozzle throat was almost two times lower for the HRM case. Moreover, the difference in velocity is most significant in the diverging part of the motive nozzle. Nevertheless, the maximal velocity at the motive nozzle outlet was almost identical for both approaches. The number of sonic waves that occurred after the motive nozzle was identical for both models, but the predicted shapes were slightly different. The HRM results show a more rapid change in velocity after the first wave. In consequence, the shock-wave shape was different.

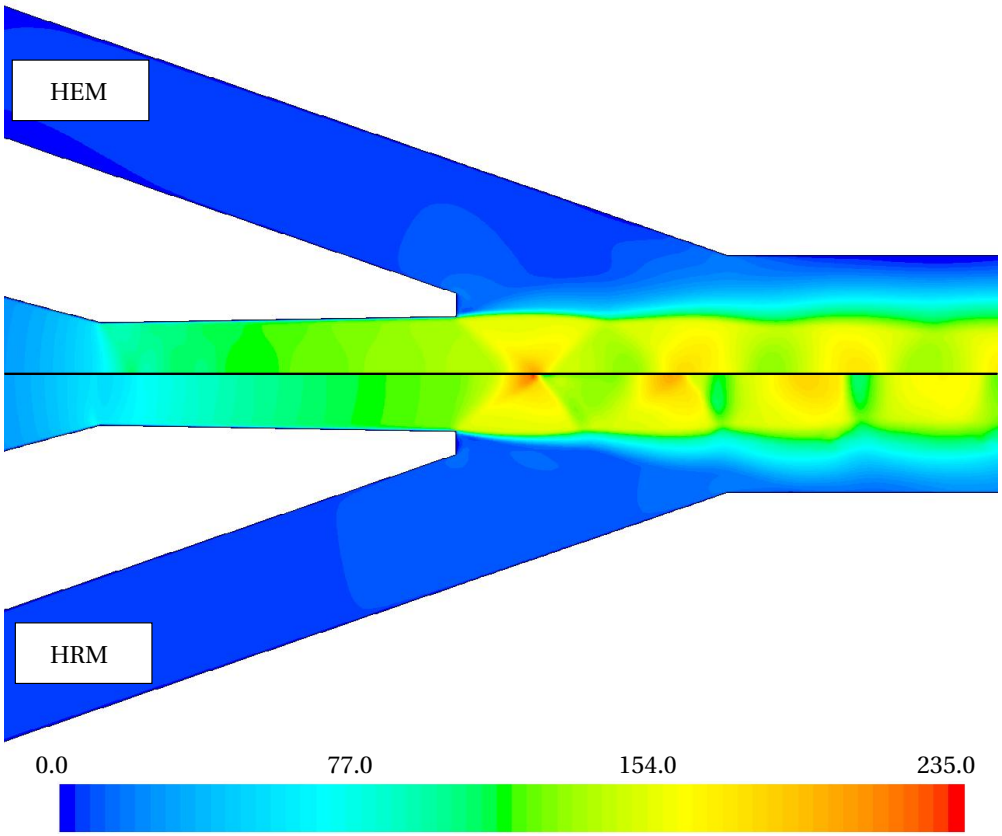

Figure 6: Velocity magnitude field for HEM (top) and HRM (bottom) in the motive nozzle and mixer inlet for OR#13

In addition to the velocity fields, the pressure fields were analysed. In Fig. 7, the computed HEM and HRM pressure fields for OR #13 in the motive nozzle diverging part and pre-mixing section were compared. Significant differences were found in the diverging part of the motive nozzle. The expansion of the primary fluid in the HRM approach was more rapid for the HEM computations. Moreover, the lowest pressure in the ejector, namely the pre-mixing chamber, was noted for the equilibrium model. Consequently, the HRM had a smoother pressure profile than the HEM. Nevertheless, the absolute pressure in crucial parts of the motive nozzle, i.e., motive nozzle inlet, motive nozzle throat and motive nozzle outlet, was at the identical level for both modes. The predicted area-weighted average absolute pressure at the mentioned cross-sections for both models is presented in Table 3. The difference between the HEM and HRM results at the selected cross-sections can be considered negligible. Hence, the pressure drop that caused the suction was similar for both models. However, the HRM had higher suction nozzle mass flow rates than the HEM. This increase is a result of the increased motive nozzle mass flow rate. Considering the accuracy of the motive nozzle mass flow rate prediction in Fig. 2, and χ prediction in Fig. 3, we notice that the small error of the motive nozzle mass flow rate does not necessarily result in a low χ error.

Table 3: Area-weighted average absolute pressure at the motive nozzle cross-sections

Cross-section	HEM, bar	HRM, bar
Motive nozzle inlet	78.1	78.1
Motive nozzle throat	61.8	62.2
Motive nozzle outlet	33.9	33.2

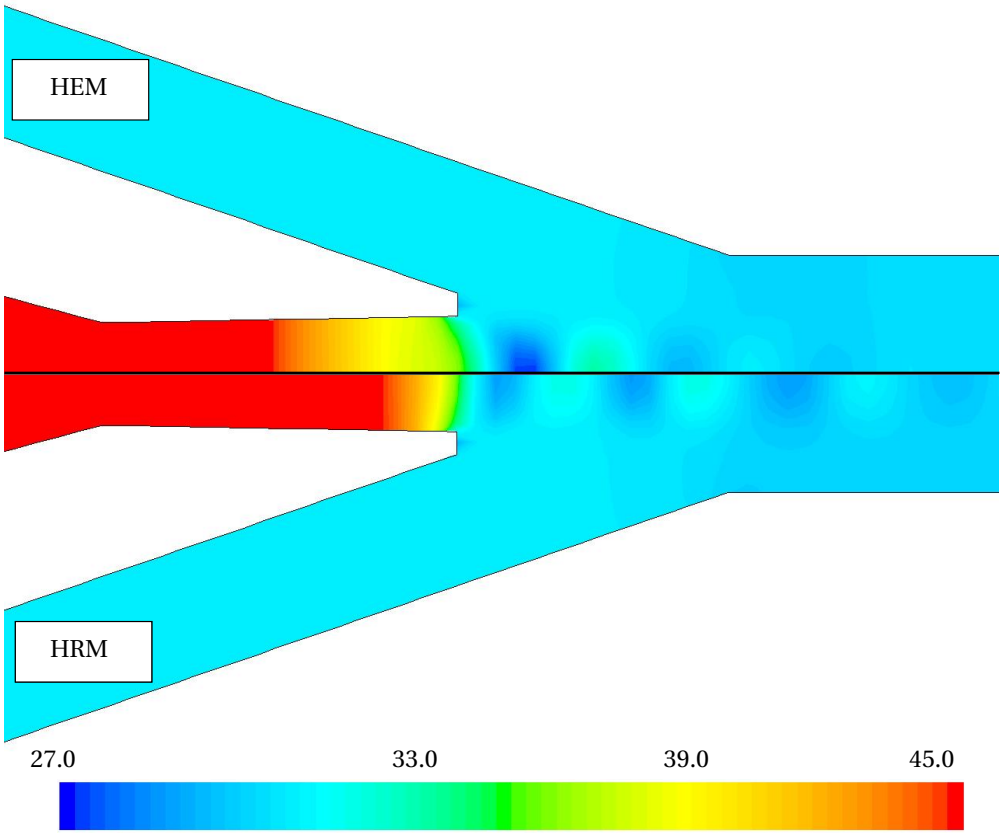

Figure 7: Absolute pressure field (bar) for HEM (top) and HRM (bottom) in the motive nozzle and mixer inlet for OR#13

5. Conclusions

The accuracy of two selected two-phase flow models was analysed in this paper: the homogeneous equilibrium model and homogeneous relaxation model. The models were analysed in terms of the operating regime characteristic for a supermarket refrigeration system. The range of the investigated motive nozzle inlet conditions was typical for refrigeration systems in the northern and southern parts of Europe. The motive nozzle inlet pressure was 47 bar to 95 bar, and the temperature was 6°C to 35°C. The computed mass flow rates were compared with the measured values to assess the model performance. The model results were considered accurate when the discrepancy between experimental and computed values was below ±10%. The considered models were implemented by the *ejectorPL* computational tool, which was previously used in numerous CO_2 ejector analyses.

The model evaluation showed a notably strong relation between the model accuracy and the ORs. The model accuracy tends to decrease with the decreasing pressure and temperature. The model performance was satisfactory for the motive nozzle operating conditions near the refrigerant critical point. However, the model fidelity was

poor for the motive nozzle operating regimes far below the critical point. For such conditions, the error of the simulated motive nozzle mass flow rate was significantly higher. This tendency was observed for both investigated models.

The accuracy improvements after the HRM implementation were lower than expected. The noted fidelity increase was only up to 5% for specific operating regimes. For the lowest considered motive nozzle inlet pressures and temperatures, the increase was 3%. These results show that the relaxation time formulation should be considered in future studies. For the low-pressure and -temperature conditions, θ should be significantly longer than the calculated value according to Eq. (10) which was introduced by [29]. However, time should be decreased to improve the accuracy for the operating regimes above the critical point. Considering that the θ definition in [29] was formulated for the narrow range of operating conditions in the experimental investigation in [30], the new θ formulation should be redefined to consider the range of typical nozzle operating conditions for refrigeration systems.

The effect of the motive nozzle mass flow errors on the predicted χ was also analysed. The highest mass entrainment ratio discrepancy was noted for the low-pressure and low-temperature conditions. For the lowest considered pressure, the χ equal to 0 was predicted in the HEM approach. Moreover, the analysis results show that the satisfying accuracy of the simulated primary stream mass flow rate does not guarantee an accurate prediction of mass entrainment ratio.

The HRM implementation resulted in the higher accuracy of the computations for the lower temperature and pressure. The relaxation time and delayed evaporation increased the density of the expanding fluid at the motive nozzle throat. In consequence, the motive nozzle mass flow rate increased. This modification improved the accuracy compared to HEM in terms of the motive nozzle mass flow rate prediction. Nevertheless, for some operating conditions, the χ accuracy decreased after the HRM model was applied. Moreover, the HRM had lower accuracy than the HEM for the operating regimes above the critical point

The detailed analysis of the flow profiles and flow fields shows differences between the HEM and HRM computations. Because of the relaxation time introduced to HRM, the evaporation of the fluid was delayed compared to HEM. As expected, this delay was more significant for the operating regimes far below the critical points. Thus, for the ORs, the metastability phenomenon plays the most significant role.

Acknowledgments

The authors gratefully acknowledge financial support partially from the Polish Norwegian Research Fund through project No. Pol-Nor/196445/29/2013 and partially from Research Council of Norway through project No. 244009/E20.

References

[1] G. Lorentzen, Throttling, the internal haemorrhage of the refrigeration process, Institute of Refrigeration.
[2] D. Li, E. A. Groll, Transcritical CO_2 refrigeration cycle with ejector-expansion device, Int.J. Refrigeration 28 (5) (2005) 766 – 773.
[3] S. Elbel, P. Hrnjak, Experimental validation of a prototype ejector designed to reduce throttling losses encountered in transcritical R744 system operation, Int. J. Refrigeration 31 (2008) 411 – 422.
[4] B. T. Austin, K. Sumathy, Transcritical carbon dioxide heat pump systems: A review, Renew. Sustain. Energy Rev. 15 (8) (2011) 4013–4029. doi:10.1016/j.rser.2011.07.021.
URL http://dx.doi.org/10.1016/j.rser.2011.07.021
[5] S. Elbel, N. Lawrence, Review of recent developments in advanced ejector technology, Int. J. Refrigeration 62 (2016) 1 – 18. doi:http://dx.doi.org/10.1016/j.ijrefrig.2015.10.031.
[6] G. Besagni, R. Mereu, F. Inzoli, Ejector refrigeration: A comprehensive review, Renew. Sust. Eerg. Rev. 53 (2016) 373 – 407.
[7] M. Haida, K. Banasiak, J. Smolka, A. Hafner, T. M. Eikevik, Experimental analysis of the R744 vapour compression rack equipped with the multi-ejector expansion work recovery module, Int. J. Refrigeration 64 (2016) 93 – 107. doi:http://dx.doi.org/10.1016/j.ijrefrig.2016.01.017.
[8] F. Liu, E. A. Groll, J. Ren, Comprehensive experimental performance analyses of an ejector expansion transcritical CO_2 system, App. Therm. Eng. 98 (2016) 1061 – 1069.
[9] K. Banasiak, A. Hafner, E. E. Kriezi, K. B. Madsen, M. Birkelund, K. Fredslund, R. Olsson, Development and performance mapping of a multi-ejector expansion work recovery pack for R744 vapour compression units, Int. J. Refrigeration.
[10] J. Smolka, M. Palacz, J. Bodys, K. Banasiak, A. Fic, Z. Bulinski, A. J. Nowak, A. Hafner, Performance comparison of fixed- and controllable-geometry ejectors in a CO_2 refrigeration system, Int. J Refrigeration 65 (2016) 172 – 182.

[11] F. Liu, E. A. Groll, D. Li, Investigation on performance of variable geometry ejectors for CO_2 refrigeration cycles, Energy 45 (2012) 829 – 839.
[12] F. Liu, Y. Li, E. A. Groll, Performance enhancement of CO_2 air conditioner with a controllable ejector, Int. J. Refrigeration 35 (2012) 1604 – 1616.
[13] M. Palacz, J. Smolka, W. Kus, A. Fic, Z. Bulinski, A. J. Nowak, K. Banasiak, A. Hafner, CFD-based shape optimisation of a CO_2 two-phase ejector mixing section, App. Therm. Eng. 95 (2016) 62 – 69. doi:http://dx.doi.org/10.1016/j.applthermaleng.2015.11.012.
[14] K. Banasiak, M. Palacz, A. Hafner, Z. Bulinski, J. Smolka, A. J. Nowak, A. Fic, A CFD-based investigation of the energy performance of two-phase R744 ejectors to recover the expansion work in refrigeration systems: An irreversibility analysis, Int. J. Refrigeration 40 (2014) 328 – 337.
[15] J. Sierra-Pallares, J. G. del Valle, P. G. Carrascal, F. C. Ruiz, A computational study about the types of entropy generation in three different R134a ejector mixing chambers, Int. J. Refrigeration 63 (2016) 199 – 213. doi:http://dx.doi.org/10.1016/j.ijrefrig.2015.11.007.
[16] A. A. Kornhaouser, The use of an ejector as a refrigerant expander, Inetrnational Refrigeration and Air Conditioning Conference.
URL http://docs.lib.purdue.edu/iracc/82
[17] K. Banasiak, A. Hafner, 1D computational model of a two-phase R744 ejector for expansion work recovery, Int. J. Therm. Sci. 50 (2011) 2235 – 2247.
[18] A. Attou, J. Seynhaeve, Steady-state critical two-phase flashing flow with possible multiple choking phenomenon, J. Loss Prev. Process Ind. 12 (1999) 347–359. doi:10.1016/S0950-4230(98)00018-7.
[19] N. Kolev, Multiphase Flow Dynamics 2: Thermal and Mechanical Interactions, Multiphase Flow Dynamics, Springer Berlin Heidelberg, 2005.
URL https://books.google.pl/books?id=xDlH10cjlckC
[20] K. Banasiak, A. Hafner, T. Andresen, Experimental and numerical investigation of the influence of the two-phase ejector geometry on the performance of the R744 heat pump, Int. J. Refrigeration 35 (6) (2012) 1617–1625. doi:10.1016/j.ijrefrig.2012.04.012.
URL http://linkinghub.elsevier.com/retrieve/pii/S014070071200093X
[21] A. Nowak, M. Palacz, J. Smolka, K. Banasiak, Z. Bulinski, A. Fic, A. Hafner, CFD simulations of transport phenomena during transcritical flow of real fluid (co_2) within ejector, Int. J. Numer Method H. 26 (3-4) (2016) 805–817, cited By 0.
[22] E. Rusly, L. Aye, W. Charters, A. Ooi, CFD analysis of ejector in a combined ejector cooling system, Int. J. Refrigeration 28 (7) (2005) 1092 – 1101. doi:http://dx.doi.org/10.1016/j.ijrefrig.2005.02.005.
[23] E. W. Lemmon, M. L. Huber, M. O. McLinden, NIST Standard Reference Database 23: Reference Fluid Thermodynamic and Transport Properties - REFPROP, National Institute of Standards and Technology, Standard Reference Data Program, Gaithersburg, 9th Edition (2010).
[24] J. Smolka, Z. Bulinski, A. Fic, A. J. Nowak, K. Banasiak, A. Hafner, A computational model of a transcritical R744 ejector based on a homogeneous real fluid approach, Appl. Math. Model. 37 (2013) 1208 – 1224.
[25] T.-H. Shih, W. W. Liou, A. Shabbir, Z. Yang, J. Zhu, A new k-ϵ eddy viscosity model for high reynolds number turbulent flows, Comput. Fluids 24 (1995) 227 – 238.
[26] C. Lucas, H. Rusche, A. Schroeder, J. Koehler, Numerical investigation of a two-phase CO_2 ejector, Int. J. Refrigeration 43 (2014) 154 – 166.
[27] M. Palacz, J. Smolka, A. Fic, Z. Bulinski, A. J. Nowak, K. Banasiak, A. Hafner, Application range of the HEM approach for CO_2 expansion inside two-phase ejectors for supermarket refrigeration systems, Int. J. Refrigeration 59 (2015) 251 – 258. doi:http://dx.doi.org/10.1016/j.ijrefrig.2015.07.006.
[28] P. Downar-Zapolski, Z. Bilicki, L. Bolle, J. Franco, The non-equilibrium relaxation model for one-dimensional flashing liquid flow, Int. J. Multiph. Flow 22 (3) (1996) 473–483. doi:10.1016/0301-9322(95)00078-X.
URL http://www.sciencedirect.com/science/article/pii/030193229500078X
[29] W. Angielczyk, Y. Bartosiewicz, D. Butrymowicz, J.-M. Seynhaeve, 1-D Modeling of Supersonic Carbon Dioxide Two-Phase Flow through Ejector Motive Nozzle, Int. Refrig. Air Cond. Conf. Purdue (2010) 1–8.
[30] M. Nakagawa, M. S. Berana, A. Kishine, Supersonic two-phase flow of CO_2 through converging-diverging nozzles for the ejector refrigeration cycle, Int. J. Refrigeration 32 (6) (2009) 1195–1202. doi:10.1016/j.ijrefrig.2009.01.015.
URL http://dx.doi.org/10.1016/j.ijrefrig.2009.01.015
[31] M. Colarossi, N. Trask, D. P. Schmidt, M. J. Bergander, Multidimensional modeling of condensing two-phase ejector flow, Int. J. Refrigeration 35 (2012) 290 – 299.
[32] D. P. Schmidt, S. Gopalakrishnan, H. Jasak, Multi-dimensional simulation of thermal non-equilibrium channel flow, Int. J. Multiph. Flow 36 (4) (2010) 284–292. doi:10.1016/j.ijmultiphaseflow.2009.11.012.
URL http://www.sciencedirect.com/science/article/pii/S030193220900192X
[33] R. Benintendi, Non-equilibrium phenomena in carbon dioxide expansion, Process Saf. Environ. Prot. 92 (2014) 47–59.
[34] S. Brown, S. Martynov, H. Mahgerefteh, C. Proust, A homogeneous relaxation flow model for the full bore rupture of dense phase CO2 pipelines, Int. J. Greenh. Gas Control 17 (2013) 349–356. doi:10.1016/j.ijggc.2013.05.020.
URL http://dx.doi.org/10.1016/j.ijggc.2013.05.020
[35] M. Haida, J. Smolka, M. Palacz, J. Bodys, A. Nowak, Z. Bulinski, A. Fic, K. Banasiak, A. Hafner, Numerical investigation of an R744 liquid ejector for supermarket refrigeration systems, THERM SCI (00) (2016) 112–112. doi:10.2298/tsci151210112h.
URL http://dx.doi.org/10.2298/tsci151210112h
[36] J. Bodys, J. Smolka, M. Palacz, M. Haida, K. Banasiak, A. J. Nowak, A. Hafner, Performance of fixed geometry ejectors with a swirl motion installed in a multi-ejector module of a {CO2} refrigeration system, Energy (2016) –doi:http://dx.doi.org/10.1016/j.energy.2016.07.037.
[37] A. Hafner, K. Banasiak, T. Herdlitschka, K. Fredslund, S. Girotto, M. Haida, J. Smolka, R744 ejector system case: Italian supermarket, spiazzo, 12th IIR Gustav Lorentzen Conference on Natural Refrigerants 2016doi:http://dx.doi.org/10.18462/iir.gl.2016.1078.
[38] A. Fluent, Ansys Fluent User's Guide, Canonsburg, PA (2011).

[39] K. Banasiak, A. Hafner, Mathematical modelling of supersonic two-phase R744 flows through converging-diverging nozzles: The effects of phase transition models, Appl. Therm. Eng. 51 (2013) 635 – 643.
[40] A. Hafner, S. Försterling, K. Banasiak, Multi-ejector concept for R-744 supermarket refrigeration, Int. J. Refrigeration 43 (2014) 1–13.
[41] S. Elbel, Historical and present developments of ejector refrigeration systems with emphasis on transcritical carbon dioxide air-conditioning applications, Int. J. Refrigeration 34 (2011) 1545 – 1561.